

# Absolute Flux Calibration of STIS MAMA Imaging Modes

---

C. R. Proffitt, T. M. Brown, B. Mobasher, and J. Davies  
January 28, 2003

---

## ABSTRACT

*The absolute flux calibration of STIS MAMA imaging modes is tested by comparison of observed and predicted count rates. As part of this work, we have derived new, wavelength-dependent aperture corrections for MAMA imaging, and have revised the NUV-MAMA imaging throughput at short wavelengths. FUV-MAMA imaging modes clearly show a time dependent sensitivity loss that is consistent with the time dependent sensitivity changes seen in G140L spectra. Once this time dependence is taken into account, count rates measured using 1" apertures for FUV 25MAMA, F25LYA, F25ND3, and F25SRF2 observations are within 5% of predictions made using the prelaunch throughput determination. However, FUV F25QTZ observations show a much larger scatter than expected from Poisson statistics. NUV-MAMA imaging modes also appear to be consistent with the time dependence observed for G230L spectra, although this effect is not as large as for the FUV-MAMA. While most NUV-MAMA imaging modes show adequate agreement with the tabulated sensitivity curve, results for the F25CN182 mode are discrepant. We suggest a revision of the short wavelength throughput of the NUV-MAMA imaging modes to fix this problem. This revision brings the results for all NUV imaging modes to within 5% of predictions.*

---

## Introduction

The primary white dwarf stars used as flux calibration targets for HST are too bright to be directly imaged with most of the filters used with the STIS/MAMA detectors. Calibration of these modes therefore requires the use of fainter secondary standards. Our approach in this report will be to convolve the measured spectral energy distributions for a

number of faint standard stars with the adopted wavelength-dependent instrument throughputs to predict the count rates for MAMA imaging observations of these stars. These predicted count rates will be compared to the actual imaging observations. We will then infer what, if any, changes to the adopted throughputs are needed to bring the predicted and observed count rates into agreement.

We will assume that the wavelength-dependent throughput of the HST Optical Telescope Assembly (OTA) is known. The throughputs of the STIS filters have been directly measured by comparing filtered and unfiltered slitless spectra of hot stars. There remain, however, uncertainties in the combined throughputs of the remaining optical surfaces and detectors in STIS. For our initial comparisons between observed and predicted MAMA imaging count rates, we will adopt the prelaunch FUV-MAMA imaging throughput curve given in the reference file h2315581o\_pht. For the NUV-MAMA, we will use the throughput curve given in the reference file j7c1059ko\_pht, which was delivered in July 1999 based on preliminary on-orbit measurements.

The calibration targets for our check of the MAMA imaging absolute sensitivities are summarized in Table 1. Four of these imaging targets are isolated field stars; the remainder are in globular clusters. In the cluster NGC 2808 we only used one UV-bright star, NGC 2808-UIT1, for which STIS spectra are available from the GO program 7436. A number of MAMA images are available for this cluster from the STIS calibration program 8511. In the cluster NGC 6681, the brightest blue horizontal branch stars give count rates in the unfiltered MAMA detectors of 100 to 300 counts/second/star, making it an excellent target for the calibration of the broad band MAMA imaging modes. Numerous exposures have been taken to provide tests of geometric distortion, of flat-fielding, and as a monitor of the full field sensitivity. As part of programs 8422 and 8849, FUV/G140L, NUV/G230L, and CCD/G430L spectra were taken through the 52X2" slit, to determine the spectral energy distribution of a number of these HB stars. The slit position chosen included a dozen hot HB stars of various effective temperatures for which copious imaging data from the full field sensitivity monitor are available. The MAMA photometry of the full field imaging data is described in a separate report by Davies & Mobasher (2003).

**Table 1.** Summary of STIS MAMA Imaging Calibration Targets.

STAR	Other Names	B mag	Spectra or Teff	STIS MAMA Imaging Modes
GRW +70°5824	EGGR 102; WD 1337+70	12.7	DA:	FUV: ND3; NUV: ND3
GD 71	EGGR 210; WD 0549+158	12.81	DAw	FUV: ND3; NUV: ND3
HZ 4	EGGR 26; WD 0352+096	14.62	DA:	NUV: MGII, CIII
HS 2027+0651		16.9	DO	FUV: LYA; NUV: CN182, CN270, MGII, CIII
NGC 2808-UIT1		16.45	SDO	FUV: QTZ; NUV: CN270
NGC 6681 a	M 70	15.95	8330 K	FUV: Clear, SRF2, QTZ; NUV: SRF2, QTZ, CN182, CN270
NGC 6681 b	“	16.21	9580 K	“
NGC 6681 c	“	16.83	12350 K	“
NGC 6681 d	“		7900 K	“
NGC 6681 g	“	16.11	10210 K	“
NGC 6681 i	“	16.78	12360 K	“
NGC 6681 j	“	15.90	8300 K	“
NGC 6681 k	“	18.36	19150 K	“
NGC 6681 l	“	14.72	8090 K	“
NGC 6681 m	“	17.16	14980 K	“

## Adopted Spectral Energy Distributions.

### *Spectral Energy Distributions of Individual Standard Stars.*

Accurate fluxes have been determined for a number of hot standards by Bohlin (2000) and by Bohlin, Dickinson, & Calzetti (2001). Updated versions of these spectra have recently been provided by Bohlin (private communication), and we have adopted these spectral energy distributions for the stars HS 2027+0651, GRW +70°5824, HZ 4, and GD 71. For the star NGC 2808-UIT1, we used G140L, G230L, and G430L observations from the GO program 7436 (Wayne Landsman PI). Spectral energy distributions were determined from these spectra using the STSDAS x1d extraction task with default parameters, and these spectra were corrected for changes in sensitivity with time and temperature using an algorithm supplied by Ralph Bohlin and based on the results described in Bohlin (1999).

**Table 2.** STIS spectra of NGC 2808-UIT1 from program 7463 used in this investigation.

Rootname	Exposure time (s)	Grating	Start time
O4ER02010	1700.00	G430L	Apr 20 1999 20:54:45
O4ER02020	1700.00	G430L	Apr 20 1999 21:24:59
O4ER02030	1200.00	G140L	Apr 20 1999 22:00:05
O4ER02040	1200.00	G140L	Apr 20 1999 22:22:28
O4ER02050	1200.00	G230L	Apr 20 1999 22:50:21
O4ER02060	1200.00	G230L	Apr 20 1999 23:12:44

***Spectral Energy Distributions of Hot Stars in NGC 6681.***

On June 21, 2000, spectra and images were taken through the 52X2" slit of a number of hot HB stars in NGC 6681 as visit 6 of STIS/CAL program 8422 (Table 3). Additional spectral observations were obtained in June 2002 as part of program 8849. The slit was oriented  $307.75^\circ$  east of north and most observations were centered at RA = 18h 43m 12.6773s and DEC =  $-32^\circ 17' 26.271''$ . The slit was shifted slightly for the G140L spectra taken in June 2000 to better center the spectra on the FUV-MAMA detector. The stars observed are listed in Table 1, and a finding chart identifying them is given in Figure 1. Other details of these observations are given in Table 3.

**Table 3.** Spectral observations of stars in NGC 6681

Rootname	Exposure time (s)	Proposal ID	Grating	Start time
O5JA06030	800.00	8422	G140L	Jun 21 2000 3:24:03
O5JA06040	800.00	8422	G140L	Jun 21 2000 3:39:46
O69U09010	1546.00	8849	G140L	Jun 18 2002 3:25:56
O69U10010	1546.00	8849	G140L	Jun 20 2002 5:08:10
O5JA06080	1360.00	8422	G230L	Jun 21 2000 5:20:48
O69U09040	2588.00	8849	G230L	Jun 18 2002 4:57:21
O69U10040	2588.00	8849	G230L	Jun 20 2002 6:41:01
O5JA06050	302.00	8422	G430L	Jun 21 2000 5:00:37
O69U09020	420.00	8849	G430L	Jun 18 2002 3:56:46
O69U10020	420.00	8849	G430L	Jun 20 2002 5:39:00

For the NGC 6681 stars we have also adopted spectral energy distributions as measured by Bohlin (private communication). Spectral extractions of the NGC 6681 STIS spectra were done using standard x1d software. The images taken through the slits were

used to determine the offsets in the dispersion direction. There was sufficient sky background in each image to determine the slit locations directly from the image (Figure 2). These offsets from the slit centers were then added to the SHIFTA1 value determined from the wavecal before performing each extraction. The extracted fluxes were corrected for time dependent sensitivity changes using an algorithm derived by Ralph Bohlin. The G140L spectra were also corrected for the small temperature dependence identified by Bohlin 1999, and the G430L spectra were approximately corrected for losses due to the decline in CCD charge transfer efficiency.

In the G140L spectra, the bright HB stars themselves are the only significant source of flux. Contamination of one star's light by another is probably only important for the coolest stars which become very faint at shorter wavelengths. In the G230L and G430L spectra, however, the number of faint background stars visible increases strongly with increasing wavelength. Images show that both stars d and l have another fainter star in the slit displaced along the dispersion direction. These spectra of these stars are especially likely to be contaminated. Stars e and f shown in Figure 1 are only separated by 11.6 MAMA pixels (0.3"), and this makes it difficult to completely separate the spectra or to obtain clean large aperture imaging photometry, and so we have not attempted to use these two stars in this analysis.

**Figure 1:** Finding chart for the stars in NGC 6681 observed spectroscopically with STIS. This picture is a composite of a number of NUV-MAMA F25SRF2 observations.

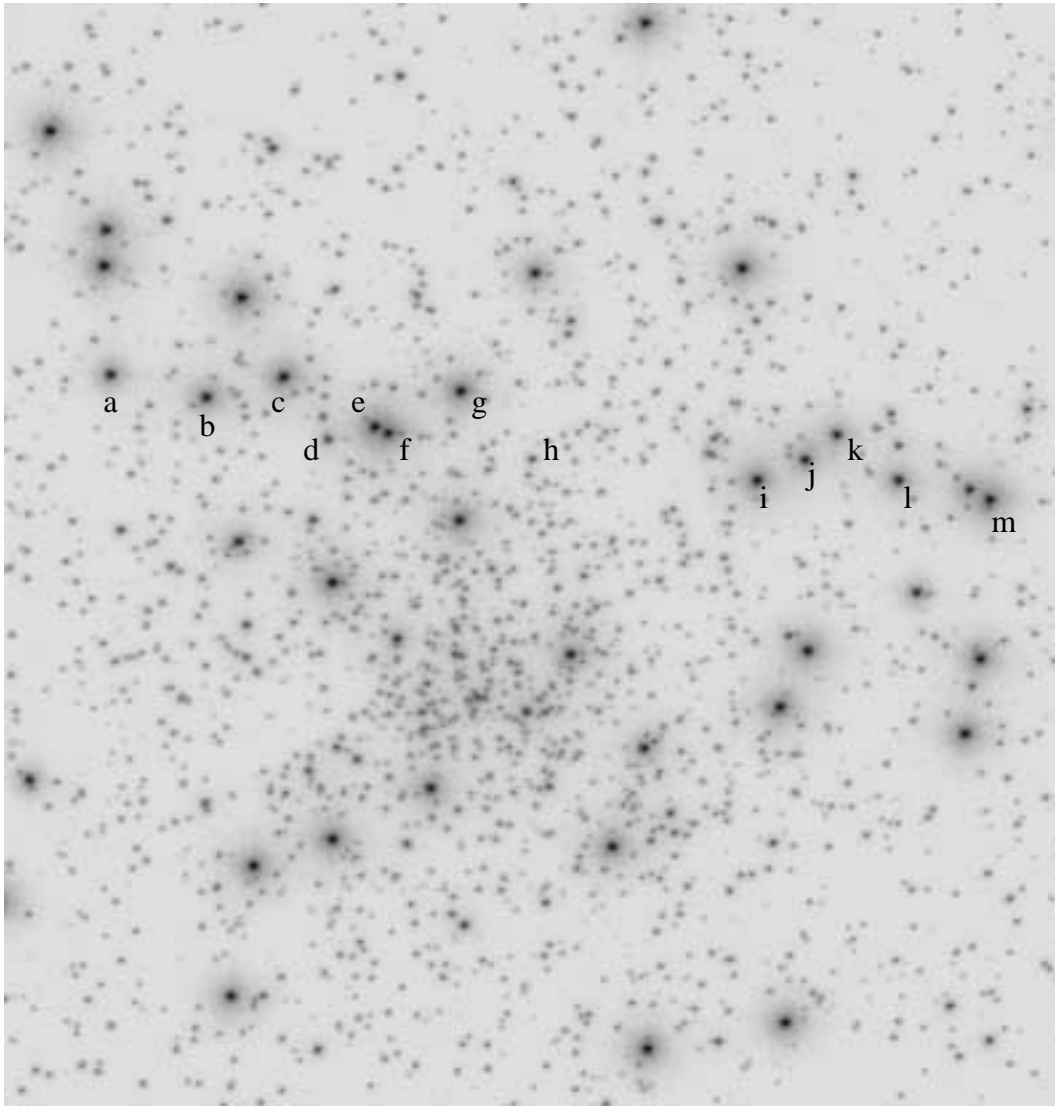
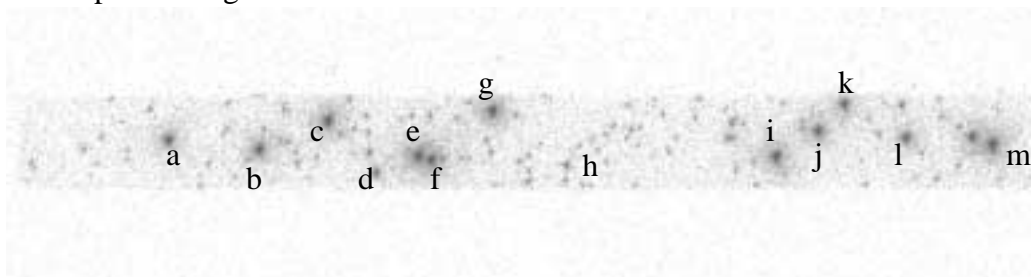


**Figure 2:** This unfiltered NUV-MAMA image (o5ja06jzq) of the NGC 6681 spectroscopic targets was taken through the 52X2 aperture and shows the positions of the individual stars within that aperture. The sky background from the cluster is sufficient to clearly define the aperture edges.



## Imaging Observations

### *MAMA Imaging of Individual Field Stars.*

The MAMA observations of individual field stars and of UIT 1 in NGC 2808 which are used here are listed in Table 4 and Table 5. Aperture photometry in instrumental magnitudes ( $-2.5 \log_{10}(\text{count rate})$ ) is summarized in Table 6. Where there are multiple observations of a given star at the same epoch, we give the mean magnitude and observation date. For NGC 2808-UIT1, nearby stars contributed to measurements with apertures larger than 20 pixels radius.

### *Aperture Corrections*

For photometry done with finite apertures, it is necessary to correct for the missing light in the wings of the PSF that fall outside the aperture. In principle, it is simple to determine the aperture corrections by observing a bright target and measuring the flux with various sized apertures. In practice, however, a noticeable fraction of the point source flux can be in a diffuse halo that can be difficult to separate from the noise and from small systematic variations in the background, and this causes additional uncertainties in the extrapolation to an idealized “infinite aperture”.

As an example, we take the broadband NUV F25ND3 images of GRW +70°5824 from visit 2 of STIS/CAL program 8422 on June 7, 2000. The F25ND3 filter is a neutral density filter with an attenuation factor of approximately 1000. After subtraction of the dark current, we find that only about 95% of the flux is contained within a 1” aperture. This differs from the encircled energy curves published by Robinson (1997) for various NUV-MAMA modes which put 98 to 99% of the flux within a 0.875” radius. However, Robinson’s results were based on images of hot horizontal-branch (HB) stars in the globular cluster NGC 6681, and due to the crowded nature of this field and the shallower images he had available, it was necessary for him to assume that all of the light was within 1.2”.

Because of the very broad band pass of most of the STIS MAMA filters, the encircled energy curve for a point source can depend strongly on the intrinsic spectral energy distribution of that source. Thus, rather than deriving a single encircled energy curve or set of aperture corrections for each filter, we will instead try to infer the appropriate aperture corrections at each wavelength and then use these to predict the aperture dependent count rates for each star and filter combination. Note, however, that MAMA imaging PSFs can change markedly between individual observations and even between different parts of the same image. This will limit the accuracy that can be obtained from individual MAMA imaging observations.

**Table 4.** NUV-MAMA Imaging Observations of Field Stars and UIT1 in NGC 2808.

filter	Target	x pos	y pos	data set	t <sub>exp</sub> (s)	start time (MJD)	40 (20) pixel instr. mag	error
F25CN182	HS 2027+0651	555.066	541.745	o4yr01kdq	144	51078.094825	-6.263	0.007
		595.634	582.363	o4yr01keq	144	51078.099351	-6.257	0.007
		473.655	460.820	o4yr01kgq	144	51078.101643	-6.267	0.007
		678.012	421.629	o4yr01kiq	144	51078.104154	-6.261	0.007
		535.021	519.461	o5ja03xiq	180	51852.256700	-6.320	0.004
F25CN270	HS 2027+0651	554.345	541.471	o4yr01kkq	240	51078.104154	-5.748	0.007
		594.977	581.855	o4yr01kmq	144	51078.107499	-5.751	0.010
		472.977	460.420	o4yr01koq	144	51078.109791	-5.758	0.010
		677.424	421.296	o4yr01kqq	144	51078.112083	-5.752	0.010
		533.908	518.849	o5ja03xfq	182	51852.252718	-5.813	0.006
	NGC 2808-UIT1	126.350	668.599	o60q03i6q	485	51562.160703	(-5.875)	0.003
		330.495	669.540	o60q03i9q	490	51562.167972	(-5.856)	0.003
		84.706	968.804	o60q53y8q	485	51594.627937	(-5.872)	0.003
		288.812	969.095	o60q53yaq	485	51594.634175	(-5.851)	0.004
		492.630	969.910	o60q53ydq	490	51594.641444	(-5.863)	0.003
F25CIII	HZ 4	86.552	565.000	o60q53yeq	490	51594.647821	(-5.863)	0.003
		86.790	767.167	o60q53yqq	490	51594.688759	(-5.867)	0.003
	HS 2027+0651	556.659	540.277	o4yr02cjq	334	51077.390022	-4.977	0.006
		597.233	580.581	o4yr02clq	240	51077.394455	-4.975	0.009
		533.590	532.737	o5ja03080[1]	300	51852.308135	-4.019	0.011
	533.635	532.814	o5ja03080[2]	300	51852.311862	-4.002	0.011	
F25MGII	HZ 4	555.154	540.133	o4yr02cgq	300	51077.383877	-4.943	0.007
		595.696	580.472	o4yr02chq	120	51077.387916	-4.952	0.011
	HS 2027+0651	534.047	519.173	o5ja03060[1]	400	51852.259385	-3.851	0.010
		534.144	519.148	o5ja03060[2]	400	51852.264269	-3.839	0.010
F25ND3	GRW +70°5824	534.687	514.861	o5ja02jfq	285	51702.347948	-4.448	0.009
		521.860	515.426	o5ja02jiq	285	51702.352902	-4.444	0.009
		547.179	527.516	o5ja02jjq	285	51702.356756	-4.464	0.009
		534.523	527.487	o5ja02jlq	285	51702.360611	-4.434	0.009
		521.833	527.582	o5ja02jmq	285	51702.364465	-4.448	0.009
		521.860	515.426	o5ja02jqq	285	51702.368319	-4.431	0.009

filter	Target	x pos	y pos	data set	t <sub>exp</sub> (s)	start time (MJD)	40 (20) pixel instr. mag	error
F25ND3	GD 71	560.561	528.231	o4dd08v6q	24	50780.241893	-4.972	0.023
		863.437	831.903	o4dd08v8q	24	50780.243885	-4.992	0.023
		867.514	228.321	o4dd08vaq	24	50780.245875	-4.986	0.023
		252.796	829.213	o4dd08vcq	24	50780.247866	-4.907	0.024
		255.094	224.236	o4dd08veq	24	50780.249856	-4.884	0.024

**Table 5.** FUV-MAMA Imaging Observations of Field Stars and NGC 2808-UIT1.

filter	Target	x pos	y pos	data set	t <sub>exp</sub> (s)	start (MJD)	40 (20) pixel instr. mag	error
F25LYA	HS 2027+0651	554.594	549.694	o5ja030b0[1]	285	51852.330924	-4.441	0.009
		554.720	549.983	o5ja030b0[2]	360	51852.367869	-4.416	0.009
F25ND3	GRW +70°5824	550.297	525.719	o5ja02k1q	326	51702.402809	-4.083	0.009
		562.940	525.645	o5ja02k7q	300	51702.407138	-4.077	0.010
		562.920	538.387	o5ja02kdq	300	51702.411166	-4.080	0.010
		550.415	538.360	o5ja02k3q	300	51702.415194	-4.085	0.010
		537.812	538.354	o5ja02k9q	300	51702.419222	-4.086	0.010
		537.690	525.851	o5ja02k5q	300	51702.423249	-4.082	0.010
	537.695	513.326	o5ja02kbq	360	51702.427277	-4.077	0.009	
	GD 71	559.780	534.764	o4dd08uiq	24	50780.197102	-4.992	0.022
		866.347	840.495	o4dd08ukq	24	50780.199556	-4.993	0.022
		868.834	231.770	o4dd08uzq	24	50780.234475	-5.051	0.022
252.762		839.105	o4dd08v1q	24	50780.236466	-5.003	0.022	
252.322	839.343	o4dd08v3q	24	50780.238387	-4.966	0.023		
F25Q TZ	NGC 2808-UIT1	135.07	662.58	o60q02f8q	538	51561.160321	(-6.167)	0.003
		340.68	663.16	o60q02fbq	480	51561.196664	(-6.135)	0.003
		271.49	951.08	o60q52kxq	538	51590.732613	(-6.204)	0.003
		476.34	951.63	o60q52l0q	480	51590.740495	(-6.136)	0.003
		66.07	543.46	o60q52l1q	500	51590.746756	(-6.098)	0.003
		66.10	746.60	o60q52l3q	500	51590.753168	(-6.136)	0.003

**Table 6.** Mean measured instrumental magnitudes for field stars and NGC 2808-UIT1 as a function of aperture radius in detector pixels.

Detector	aperture	target	date	5	10	15	20	40	80
NUV	F25CN182	HS 2027+0651	1998.73	-5.814	-5.979	-6.072	-6.143	-6.261	-6.306
			2000.84	-5.879	-6.037	-6.132	-6.202	-6.319	-6.361
	F25CN270	HS 2027+0651	1998.73	-5.426	-5.556	-5.627	-5.669	-5.752	-5.797
			2000.84	-5.483	-5.621	-5.688	-5.729	-5.812	-5.855
		NGC 2808-UIT1	2000.11	-5.548	-5.746	-5.819	-5.867	...	...
	F25CIII	HS 2027+0651	2000.84	-3.549	-3.716	-3.809	-3.880	-4.011	-4.062
			HZ 4	1998.72	-4.520	-4.677	-4.772	-4.839	-4.976
	F25MGII	HS 2027+0651	2000.84	-3.514	-3.651	-3.720	-3.761	-3.844	-3.883
			HZ 4	1998.72	-4.626	-4.760	-4.832	-4.872	-4.947
	F25ND3	GRW +70°5824	2000.43	-4.033	-4.192	-4.287	-4.345	-4.445	-4.491
			GD 71 <sup>1</sup>	1997.91	-4.533	-4.700	-4.794	-4.849	-4.972
FUV	F25LYA	HS 2027+0651	2000.84	-3.760	-4.043	-4.200	-4.296	-4.429	-4.486
	F25ND3	GRW +70°5824	2000.43	-3.531	-3.746	-3.873	-3.960	-4.080	-4.121
			GD 71 <sup>1</sup>	1997.91	-4.421	-4.653	-4.789	-4.886	-4.992
	F25QTZ	NGC 2808-UIT1	2000.10	-5.770	-5.966	-6.072	-6.146	...	...

<sup>1</sup>For GD 71 we adopt the magnitudes from the observations that were done with the target closest to the center of the detector (o4dd08v6q and o4dd08uiq).

To derive monochromatic PSFs for the NUV and FUV-MAMA detectors we used those observations in Table 6 done with the narrow band F25LYA, F25CIII, and F25MGII filters to give a first approximation to the encircled energy curve at three wavelengths. The adopted spectral energy distribution for each star was then combined with the interpolated wavelength-dependent encircled energy curve and used as input to **synphot** tasks to predict the encircled energy curve for each star/filter/detector combination. The adopted wavelength-dependent aperture corrections were then adjusted as needed to give good agreement between the predictions and observations. We then normalized these encircled energy curves to unity for apertures of 40 pixel radius. Although it is clear that in reality a few percent of the total flux is actually outside this radius, the accuracy with which we can measure the encircled flux declines for larger aperture radii. In addition, as we will see, normalizing to 40 pixel apertures gives good agreement with the currently tabulated detector sensitivity and filter throughput curves for most modes. The final adopted monochromatic encircled energy curves are given in Table 7 in the form of aperture corrections:  $2.5 \cdot \log_{10}(\text{encircled energy fraction})$ , normalized to unity at a 40 pixel radius. In Figure 3, we compare these wavelength-dependent aperture corrections with the narrow band filter measurements. The detailed shape of the wavelength-dependent aperture cor-

rections are most uncertain between 1300 and 1700 Å, where they appear to be changing rapidly as a function of wavelength.

**Figure 3:** Solid lines show the adopted wavelength-dependent aperture corrections for 5, 10, 15, and 20 pixel apertures. The open symbols show the measured aperture corrections for narrow band F25CIII and F25MGII observations of the hot standard star HZ 4 and F25LYA observations of HS 2027+0651. All values shown here are normalized to an aperture correction of unity for a 40 pixel aperture.

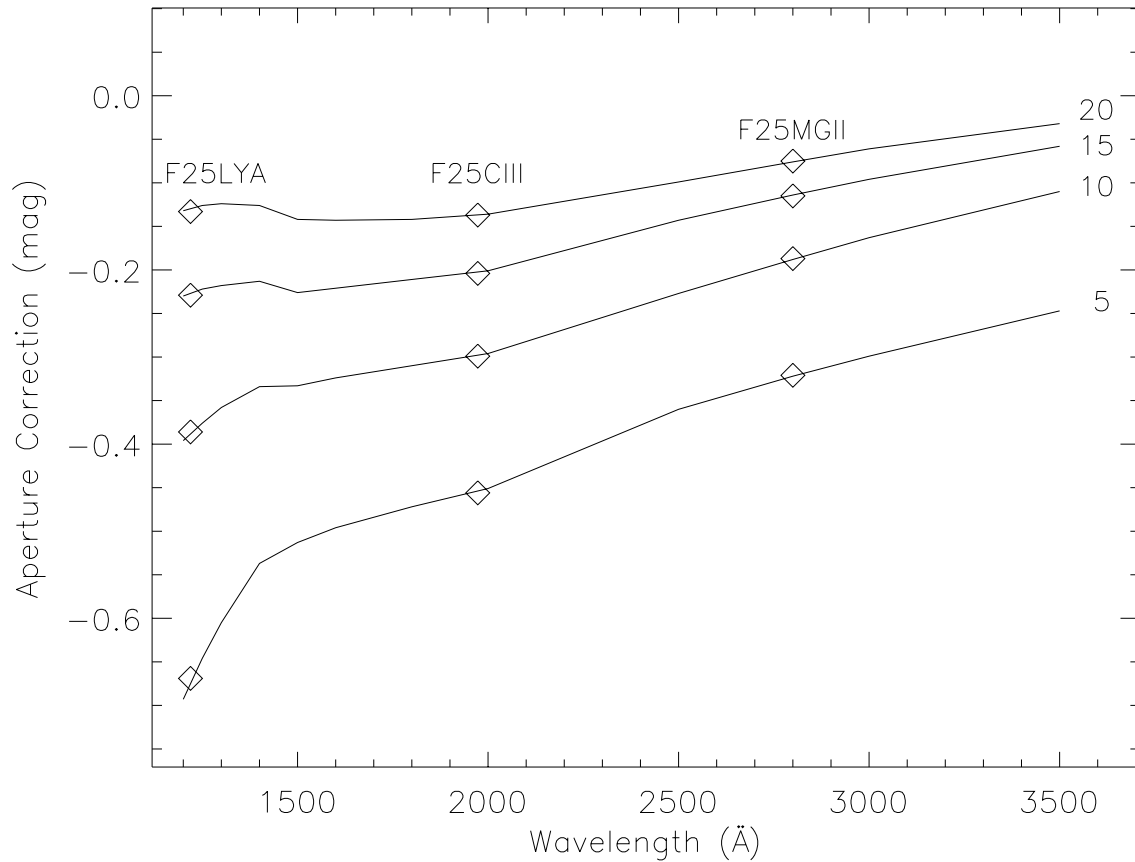


**Table 7.** Adopted monochromatic aperture corrections vs. aperture radius normalized to unity for a 40 pixel radius aperture.

Aperture radii in pixels								
$\lambda$ (Å)	3	5	7	10	15	20	40	80
Aperture Correction in Magnitudes								
1200	-1.106	-0.693	-0.546	-0.396	-0.230	-0.132	0	+0.058
1250	-0.982	-0.646	-0.511	-0.376	-0.222	-0.126	0	+0.053
1300	-0.916	-0.605	-0.482	-0.358	-0.218	-0.124	0	+0.050
1400	-0.809	-0.537	-0.438	-0.334	-0.213	-0.126	0	+0.044
1500	-0.777	-0.513	-0.427	-0.333	-0.226	-0.142	0	+0.040
1600	-0.755	-0.496	-0.413	-0.324	-0.221	-0.143	0	+0.040
1800	-0.724	-0.472	-0.391	-0.310	-0.211	-0.142	0	+0.040
2000	-0.694	-0.451	-0.372	-0.296	-0.201	-0.136	0	+0.041
2500	-0.569	-0.360	-0.289	-0.227	-0.143	-0.099	0	+0.048
2800	-0.491	-0.322	-0.245	-0.188	-0.114	-0.076	0	+0.053
3000	-0.446	-0.299	-0.220	-0.163	-0.096	-0.061	0	+0.055
3500	-0.421	-0.247	-0.174	-0.110	-0.058	-0.032	0	+0.051

The exact aperture correction for a given observation will depend on the source spectrum as well as on the filter and detector used. The best approach is to use the wavelength-dependent aperture corrections given in Table 7 as an additional input component when modelling a source spectrum with **synphot** in order to directly calculate a predicted count rate for a given source spectrum and aperture size. In Table 8 we give the aperture corrections calculated for spectra with constant flux per unit wavelength ( $F_\lambda = \text{constant}$ ). These latter values may be used when the source spectral energy distribution is unknown or when approximate results are adequate.

**Table 8.** Aperture corrections for individual filters calculated assuming the wavelength-dependent aperture corrections given in Table 7 and a source spectrum with  $F_\lambda = \text{constant}$ .

Detector/Filter	Aperture radii in pixels				
	3	5	10	15	20
Aperture Correction in Magnitudes					
NUV F25CIII	-0.680	-0.441	-0.287	-0.194	-0.130
NUV F25CN182	-0.664	-0.431	-0.279	-0.186	-0.123
NUV F25ND3	-0.561	-0.365	-0.223	-0.141	-0.093
NUV F25SRF2	-0.578	-0.375	-0.232	-0.149	-0.099
NUV F25QTZ	-0.572	-0.371	-0.230	-0.147	-0.099
NUV F25CN270	-0.512	-0.332	-0.198	-0.121	-0.082
NUV F25MGII	-0.485	-0.316	-0.182	-0.110	-0.073
FUV F25LYA	-1.030	-0.651	-0.381	-0.227	-0.127
FUV 25MAMA	-0.855	-0.556	-0.340	-0.214	-0.122
FUV F25ND3	-0.851	-0.554	-0.339	-0.214	-0.120
FUV F25SRF2	-0.785	-0.515	-0.323	-0.210	-0.120
FUV F25QTZ	-0.752	-0.494	-0.321	-0.218	-0.132

*Comparison of observed and predicted count rates.*

We will assume that the time dependent changes in the throughputs of the MAMA imaging modes are the same as that found for the MAMA low dispersion spectral modes (Bohlin 1999; Stys & Walborn 2001). Because aperture corrections and the rate of sensitivity change varies significantly with wavelength, we apply the wavelength-dependent aperture corrections and the sensitivity changes at a given time to each adopted target spectrum, and then use the **calphot** routine in the STSDAS **synphot** package to determine the predicted count rate for a given filter-detector combination for each aperture size.

Table 9 compares predicted and observed magnitudes for each of the entries in Table 6. Except for some of the later epoch (2000.84) data for HS 2027+0651, all 40 pixel aperture measurements (for which the aperture corrections are defined to be zero) agree with predictions to better than five percent. For both the F25CN182 and the F25CN270 filters, the instrumental magnitudes measured in the year 2000 for HS 2027+0651 are several percent brighter than the 1998 measurements. The NGC 6681 observations done using this filter are not consistent with this large a change in the time dependent sensitivity, so data for this star should be treated with caution.

**Table 9.** Predicted - observed magnitudes (defining 40 pixel aperture correction as unity).

detector	filter	target	date	Aperture radius in pixels					
				5	10	15	20	40	80
NUV	F25ND3	GRW +70°5824	2000.43	-0.044	-0.039	-0.035	-0.037	-0.044	-0.045
	F25ND3	GD 71	1997.91	-0.029	-0.022	-0.023	-0.032	-0.018	-0.024
	F25CIII	HS 2027+0651	2000.84	+0.036	+0.047	+0.045	+0.049	+0.047	+0.057
	F25CIII	HZ 4	1998.72	+0.021	+0.023	+0.024	+0.026	+0.031	+0.035
	F25MGII	HS 2027+0651	2000.84	+0.005	+0.008	+0.003	+0.006	+0.014	-0.000
	F25MGII	HZ 4	1998.72	-0.028	-0.028	-0.029	-0.027	-0.026	-0.031
	F25CN182	HS 2027+0651	1998.73	-0.007	-0.002	-0.007	-0.006	-0.016	-0.014
	F25CN182	HS 2027+0651	2000.84	+0.089	+0.087	+0.085	+0.084	+0.073	+0.073
	F25CN270	HS 2027+0651	1998.73	-0.017	-0.020	-0.026	-0.024	-0.024	-0.030
	F25CN270	HS 2027+0651	2000.84	+0.061	+0.066	+0.056	+0.057	+0.057	+0.049
	F25CN270	NGC 2808-UIT1	2000.11	-0.064	+0.000	-0.004	+0.005	...	...
FUV	F25LYA	HS 2027+0651	2000.84	-0.006	+0.009	+0.013	+0.009	+0.017	+0.016
	F25ND3	GRW +70°5824	2000.43	+0.016	+0.018	+0.023	+0.017	+0.020	+0.008
	F25ND3	GD 71	1997.91	-0.001	+0.007	+0.014	+0.016	+0.004	-0.015
	F25QTZ	NGC 2808-UIT1	2000.10	-0.071	-0.049	-0.046	-0.059	...	...

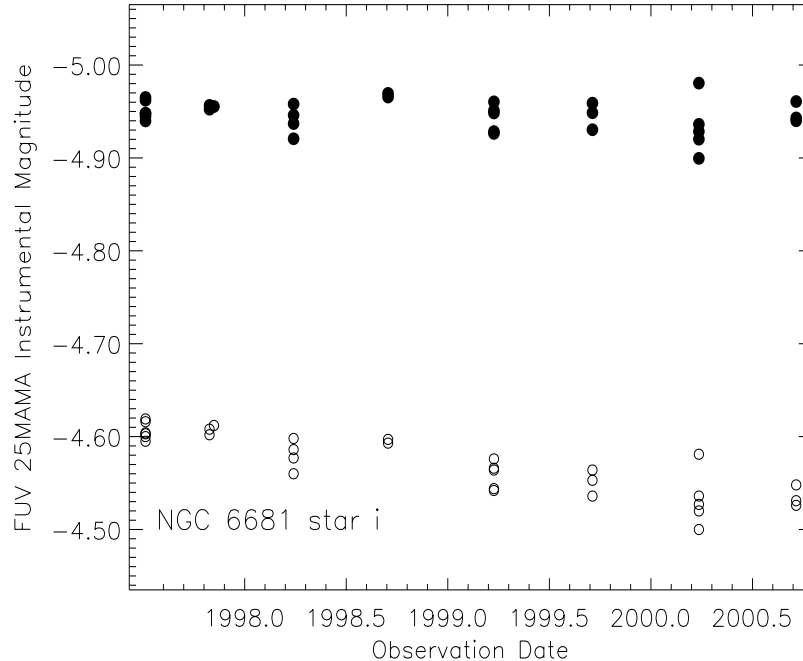
### *NGC 6681 Imaging Observations*

The globular cluster NGC 6681 contains a large number of hot horizontal branch stars that are faint enough to observe safely with any STIS MAMA imaging mode, but bright enough to give good S/N in a short exposure. This cluster is observed every six months as a full field check of the MAMA imaging mode throughputs (STIS/CAL programs 7080, 7132, 7720, 7788, 8425, 8858, and 8918). During each visit, NUV-F25SRF2 and FUV-25MAMA images are taken at four different pointings separated by 10", and NUV-F25QTZ, NUV-F25CN182, NUV-F25QTZ, NUV-F25CN182, FUV-F25QTZ, and FUV-F25SRF2 images are each taken at a single pointing. Davies & Mobasher have described the analysis of these full field data and we will adopt their photometry for comparison with the count rates predicted from the adopted spectral energy distributions.

Because of the strong variation of the time dependence of the sensitivity with wavelength for the FUV-MAMA, we cannot simply use the average observed magnitude for each star. An example of the effects of these time dependent sensitivity changes and the corrections for a finite aperture size is shown in Figure 4. For this figure we calculated a predicted count rate for each observation both with and without the time dependent sensi-

tivity correction and aperture corrections, and used the difference between these calculations to estimate the time dependent correction for each photometric measurement.

**Figure 4:** Individual measurements of the 10 pixel radius aperture instrumental magnitudes (open symbols) for observations of star i in NGC 6681 with the FUV-MAMA clear aperture (25MAMA) are compared with the same measurements after correction for aperture throughput and time dependent sensitivity changes (filled symbols). These corrections were calculated at each observation time by using the adopted spectral energy distribution for the star.



Relatively hot stars like NGC 6681-i show a 2% per year average decline in detected count rates when observed with the unfiltered FUV-MAMA, while cooler stars or stars observed with the FUV-QTZ long-pass filter show as much as 2.5% per year decline. We again assume that these changes in the imaging sensitivity with time for the FUV and NUV detectors have the same wavelength-dependence as the STIS G140L and G230L spectral modes respectively (Bohlin 2000). For FUV-MAMA observations we will also assume that the small temperature dependent correction found by Bohlin (1999) should be applied.

For the rest of our comparisons we will correct the predicted count rates to match the time and temperature of each individual observation. For each of the MAMA detector/filter combinations used to observe NGC 6681, the comparison between observed and predicted photometry is shown in Figure 5 through Figure 11. Observed magnitudes are taken from the full-field sensitivity monitor measurements of Davies & Mobasher for various aperture sizes. Because of the large scatter in the individual photometric

measurements, we plot only the mean value of the predicted minus the observed magnitudes for each star in these figures.

**Figure 5:** The mean difference between the predicted and observed instrumental magnitudes for FUV 25MAMA (unfiltered) observations of NGC 6681 are plotted for each star as a function of color. The comparison is made for aperture sizes of 5 (diamond symbols), 10 (+), 15 (triangles), and 20 (X) pixels radius. Stars are labeled by the identification letters given in Table 1 and Figure 1. The results for the FUV-MAMA F25ND3 filtered observations of GRW +70°5824 and GD 71 are also shown for comparison.

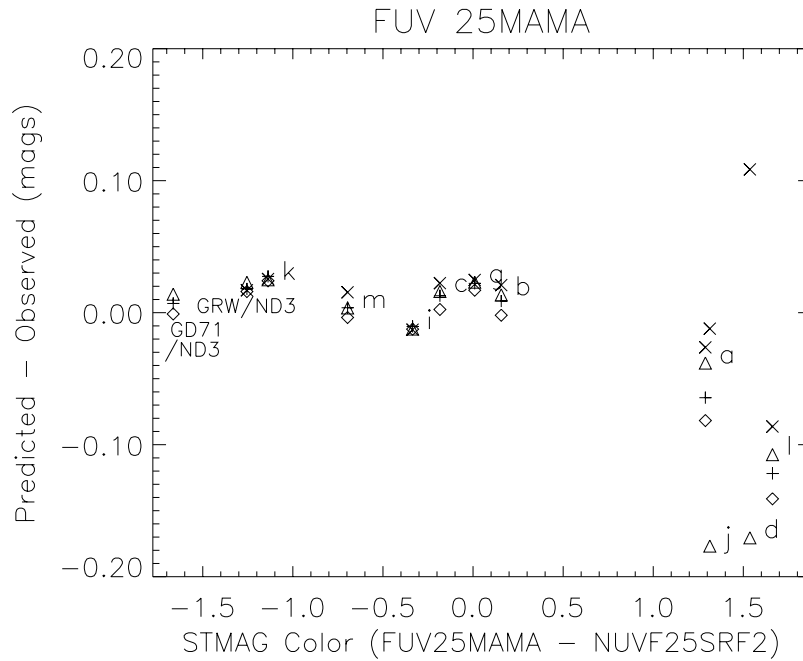


**Figure 6:** The difference between predicted and observed magnitudes for FUV F25SRF2 observations of NGC 6681. The symbols have the same meaning as in Figure 5.

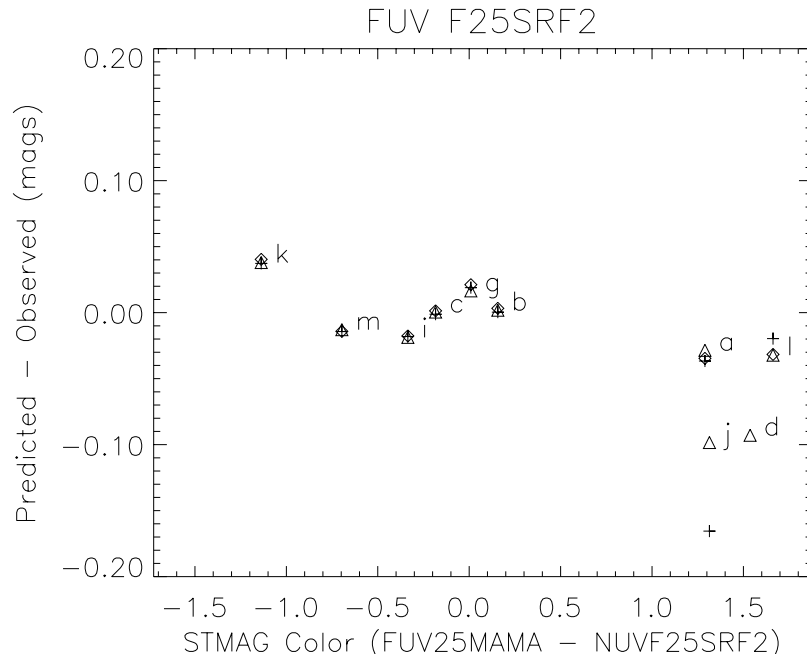


**Figure 7:** The difference between predicted and observed magnitudes for FUV F25QTZ observations of NGC 6681. The symbols have the same meaning as in Figure 5. The results for the FUV-MAMA F25QTZ observation of UIT1 in NGC 2808 are also shown.

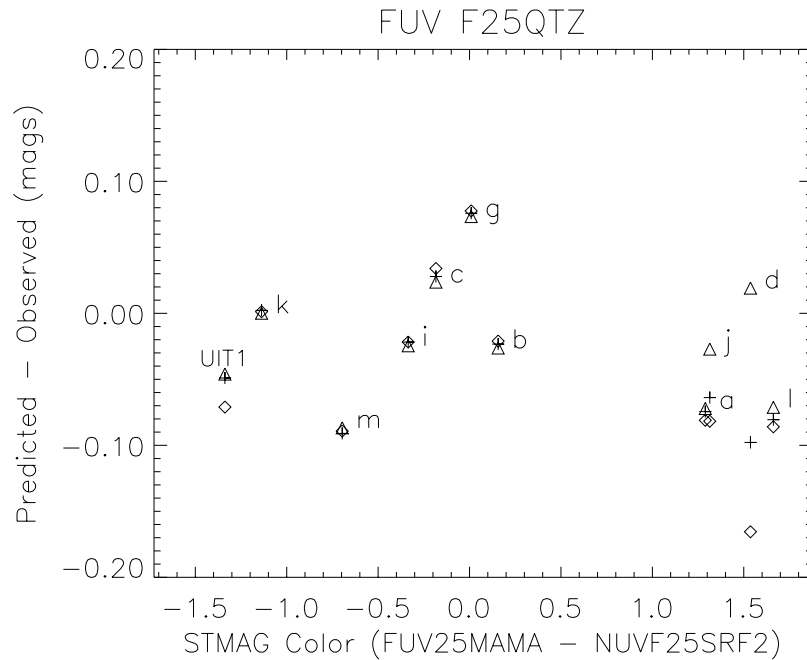


**Figure 8:** The difference between predicted and observed magnitudes for NUV-MAMA F25CN182 observations of NGC 6681. The symbols have the same meaning as in Figure 5. The results for observations of HS 2027+0651 with this filter are also shown.

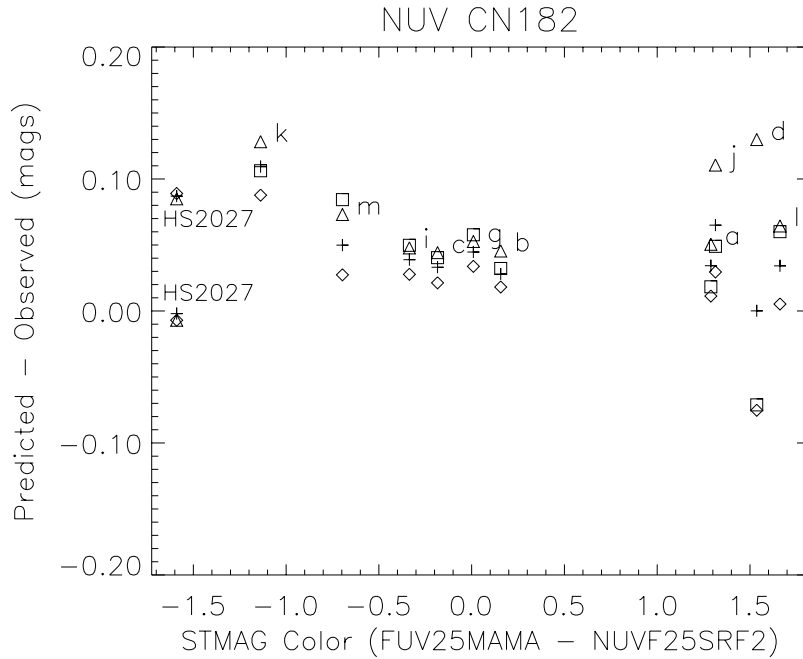


**Figure 9:** The difference between predicted and observed magnitudes for NUV-MAMA F25CN270 observations of NGC 6681. The symbols have the same meaning as in Figure 5. The results for observations of HS 2027+0651 and UIT1 in NGC 2808 with this filter are also shown.

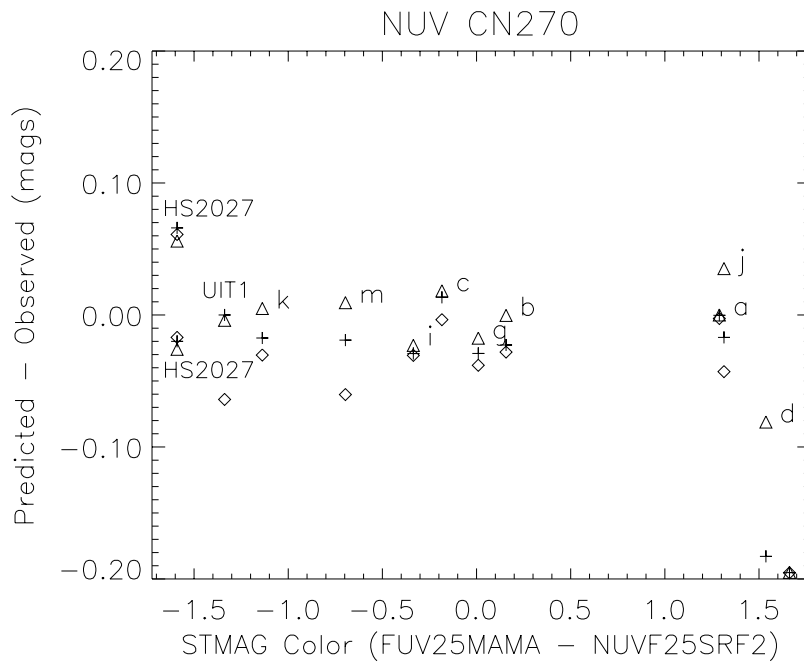


**Figure 10:** The difference between predicted and observed magnitudes for NUV-MAMA F25QTZ observations of NGC 6681. The symbols have the same meaning as in Figure 5.

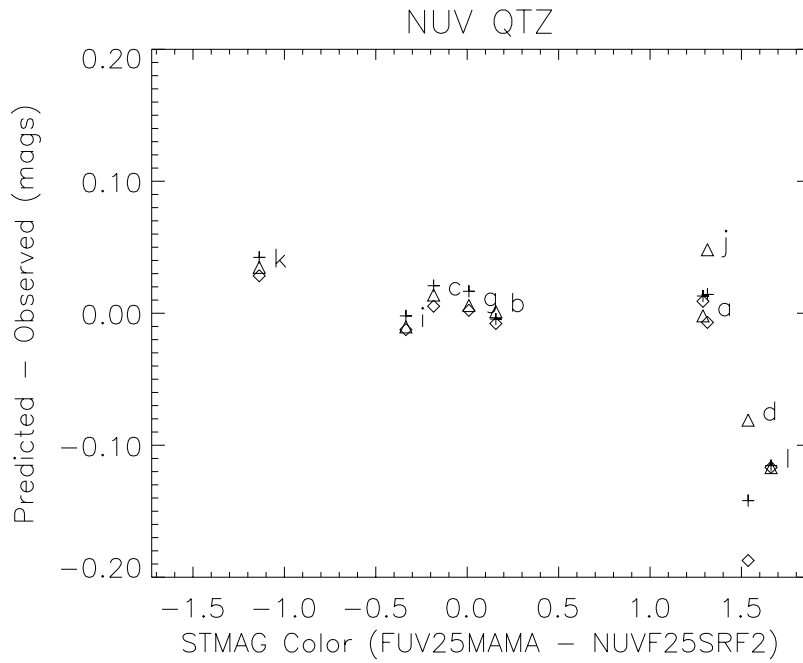
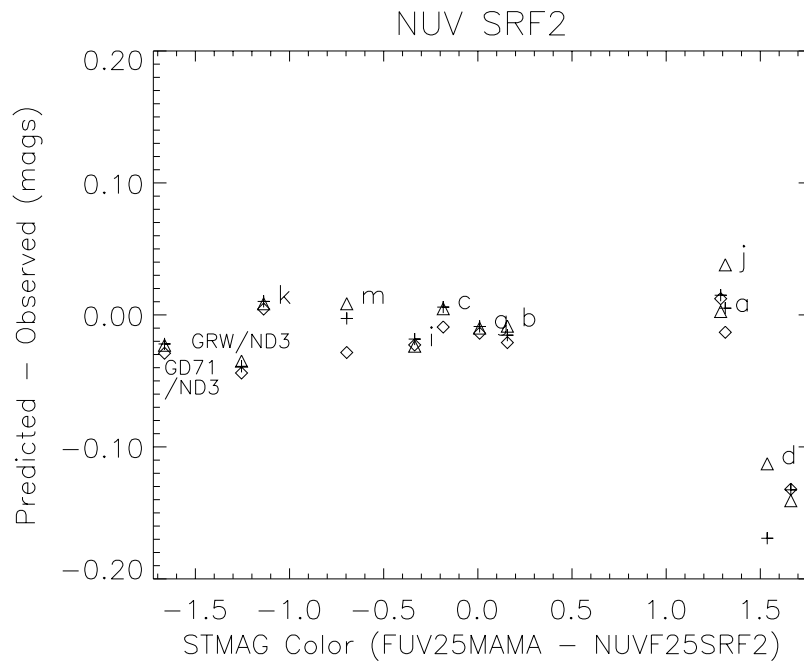


**Figure 11:** The difference between predicted and observed magnitudes for NUV-MAMA F25SRF2 observations of NGC 6681. The symbols have the same meaning as in Figure 5 on page 16. Results are also shown for the NUV-MAMA F25ND3 observations of GD 71 and GRW +70°5824.



## Discussion

### *FUV-MAMA Imaging Throughput*

The FUV-MAMA F25LYA observations of HS 2027+0651 are about 1.3% brighter than the predictions, the FUV F25ND3 observations of GD 71 and GRW +70°5824 are 2% brighter, and the F25QTZ observations of UIT1 in NGC 2808 average about 5% fainter than the predicted value. Note also that the UIT1 F25QTZ imaging observations were all significantly offset from the center of the field of view, and the individual measurements show an rms scatter of about 3%, or 10 times larger than the expected statistical error. Davies & Mobasher also found position dependent variations of as much as 10% in the brightness of other stars measured in the NGC 2808 FUV QTZ imaging data.

The comparison of the predicted and observed magnitudes for the FUV imaging observations of NGC 6681 done with the unfiltered 25MAMA aperture (Figure 5) and the F25SRF2 filter (Figure 6) show a relatively small scatter for the stars hotter than 9500 K. For the coolest stars, especially stars d and l, the predicted magnitudes are systematically too bright for a number of imaging modes. This is most likely due to difficulties in correcting for contamination from neighboring stars in the spectral observations. The scatter for all the FUV F25QTZ observations is large, but the mean observed values are about equal to predictions.

Table 10 summarizes the results discussed above. For the NGC 6681 observation we give the mean observed – predicted magnitude for stars a, b, c, g, i, k, and m. We adopt the results for the 15 pixel aperture size for this table, and exclude the three coolest stars, d, j and l, from the mean both because of their large scatter and the blended nature of their spectra. For the field star observations (and UIT1) we also adopt the 15 pixel aperture results.

**Table 10.** Mean predicted - observed magnitudes for FUV-MAMA imaging observations. Results for NGC 6681 are the mean of those for stars a, b, c, g, i, k, and m.

FUV filter	pred.-obs. (mag)
NGC 6681 mean results	
25MAMA	+0.004
F25SRF2	-0.001
F25QTZ	-0.016
Field star and UIT1 mean results	
F25LYA	+0.013
F25QTZ	-0.046
F25ND3	+0.019

***NUV-MAMA Imaging Throughput***

For most of the field star NUV-MAMA observations listed in Table 9, the agreement between the observed and predicted magnitudes is very good (1 to 3%), but there are some obvious exceptions. Results are summarized in Table 11, which has the same format as Table 10. All results refer to 15-pixel apertures and stars d, j, and l are again excluded from the mean results quoted for NGC 6681.

**Table 11.** Mean predicted - observed magnitudes for NUV-MAMA imaging observations. Results for NGC 6681 are the mean of those for stars a, b, c, g, i, k, and m. The results in the middle column assume the standard (July 1999) throughput curve for the detector. Those in the last column adopt the revised throughput illustrated in Figure 12 on page 22.

NUV Filter	pred.-obs. (mag)	revised pred.-obs. (mag)
NGC 6681 mean results		
F25SRF2	-0.003	-0.007
F25QTZ	+0.007	-0.006
F25CN182	+0.063	+0.021
F25CN270	-0.001	-0.001
Field star and UIT1 mean results		
F25ND3	-0.029	-0.009
F25CN182	+0.039	-0.005
F25CN270	+0.009	+0.009
F25MGII	+0.014	+0.014
F25CIII	+0.039	-0.015

The F25CN182 filter is especially problematic. The mean discrepancy for the F25CN182 filter is about 6% in the NGC 6681 observations, and the results for the two F25CN182 observations of HS 2027+0651 are inconsistent. These problems can be ameliorated by adjusting the short wavelength throughput curve for NUV-MAMA imaging modes. If we adopt the revised curve illustrated in Figure 12, then the bulk of the NGC 6681 F25CN182 observations can be reconciled with the predictions, as can the mean of the two F25CN182 measurements of HS 2027+0651 (see Figure 13). This change also makes the NUV-MAMA F25ND3 observations of GD 71 and GRW +70°5824 more consistent with the NUV-MAMA F25SRF2 and F25QTZ observations of NGC 6681 (see Figure 14 and the last column of Table 11). A comparison of observed and predicted magnitudes when the revised throughput curve is adopted is given in Table 12 for the observations of the standard field stars and for UIT1 in NGC 2808. Reference files reflecting this revised NUV MAMA imaging throughput curve have been delivered for use with

the **calstis** pipeline and **synphot**. Note that STIS spectroscopic flux calibrations use a separate set of reference files, and this change in the adopted imaging throughput has no effect on those calibrations.

**Figure 12:** The solid line shows the throughput curve for NUV-MAMA imaging modes adopted in July 1999. The broken curve shows our suggested revision. The throughput curves shown here have not yet been multiplied by the OTA throughput.

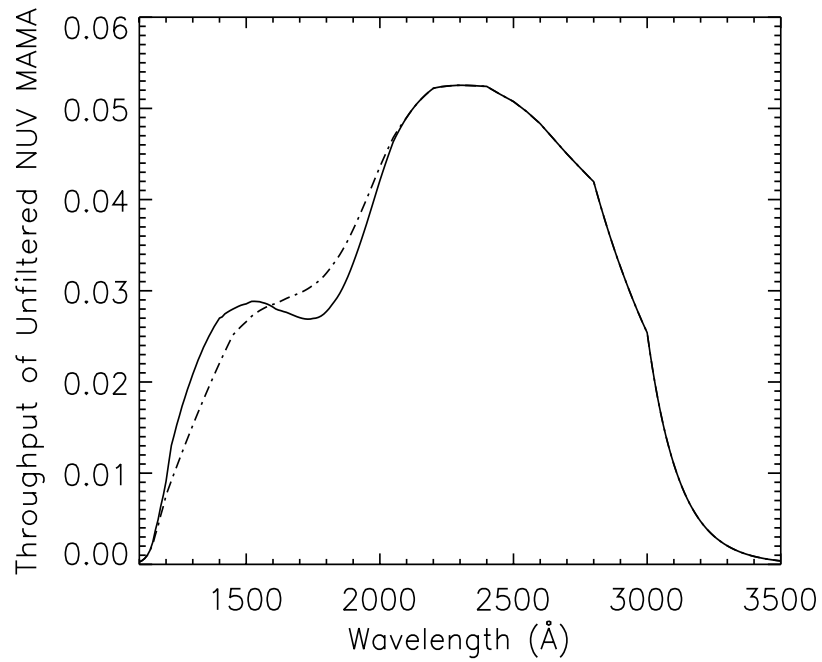


**Table 12.** Predicted minus observed magnitudes for NUV-MAMA imaging of field stars, assuming the revised NUV-MAMA throughput curve illustrated in Figure 12.

filter	target	date	Aperture radius in pixels					
			5	10	15	20	40	80
F25ND3	GRW +70°5824	2000.43	-0.028	-0.022	-0.017	-0.018	-0.025	-0.026
F25ND3	GD 71	1997.91	-0.002	0.008	0.008	0.001	0.015	0.008
F25CIII	HS 2027+0651	2000.84	-0.016	-0.005	-0.007	-0.003	-0.005	0.005
F25CIII	HZ 4	1998.72	-0.031	-0.029	-0.028	-0.027	-0.022	-0.017
F25MGII	HS 2027+0651	2000.84	0.005	0.008	0.003	0.006	0.014	0.000
F25MGII	HZ 4	1998.72	-0.028	-0.028	-0.029	-0.027	-0.026	-0.031
F25CN182	HS 2027+0651	1998.73	-0.053	-0.047	-0.051	-0.050	-0.061	-0.058
F25CN182	HS 2027+0651	2000.84	0.044	0.042	0.040	0.040	0.028	0.028
F25CN270	HS 2027+0651	1998.73	-0.017	-0.020	-0.026	-0.024	-0.024	-0.030
F25CN270	HS 2027+0651	2000.84	0.061	0.066	0.056	0.057	0.057	0.049
F25CN270	NGC 2808-UIT1	2000.11	-0.064	0.000	-0.003	0.005	...	...

**Figure 13:** The difference between predicted and observed magnitudes for NUV-MAMA F25CN182 observations of NGC 6681 when the revised NUV-MAMA throughput curve shown in Figure 12 is adopted. Results using the old throughput curve are shown in Figure 8. The symbols have the same meaning as in Figure 5.

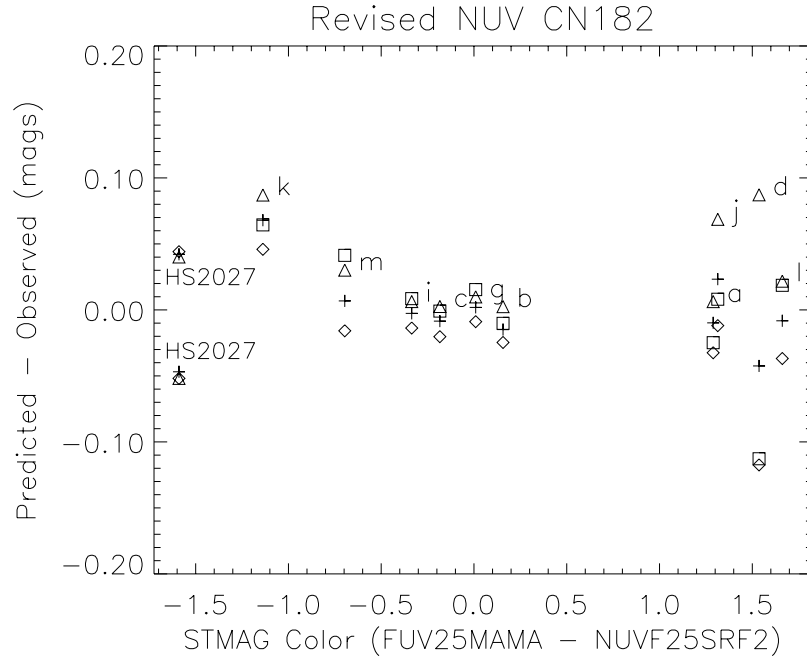
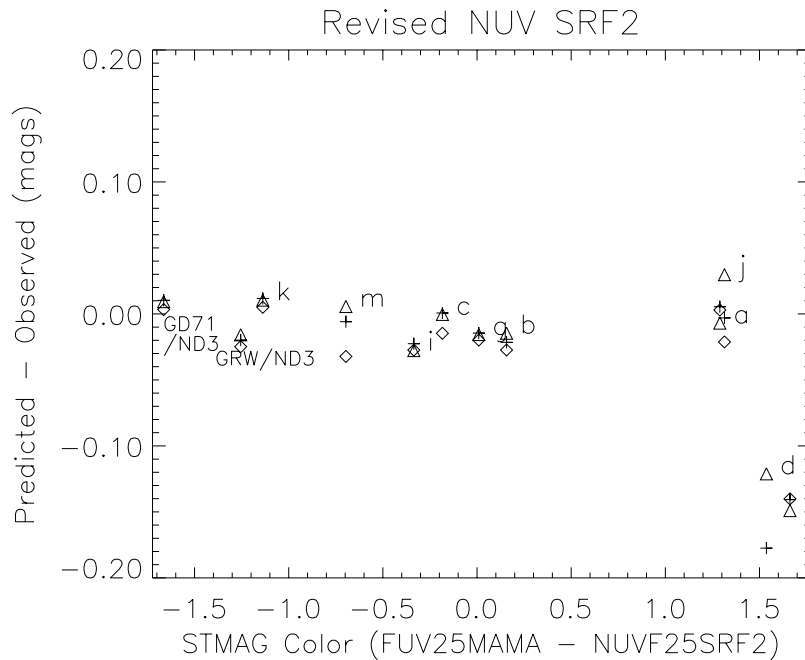


**Figure 14:** The difference between predicted and observed magnitudes for NUV-MAMA F25SRF2 observations of NGC 6681 when the revised NUV-MAMA throughput curve shown in Figure 12 is adopted (compare with Figure 11). Also shown are results for F25ND3 observations of two filed stars. Symbols have the same meaning as in Figure 5



## Conclusions

We have derived wavelength-dependent aperture corrections appropriate for STIS MAMA imaging observations of point sources, which are accurate to within 2%. If we assume that the time dependent throughput changes for the MAMA imaging modes are the same as has been determined for the low dispersion MAMA spectral modes, then combining these aperture corrections with currently tabulated throughputs for FUV-MAMA imaging modes gives absolute sensitivities which are correct to 5% or better.

For NUV-MAMA imaging modes we have derived a revised throughput curve which yields similar accuracy. This revised throughput curve is implemented in the pipeline with the reference file `n181340bo_pht.fits`, and in **synphot** with the reference file `stis_mirnuv_009_syn.fits`. These files were delivered on January 9, 2003, and only affect NUV-MAMA imaging modes.

## References

- Bohlin, R.C. 1999, STIS ISR 99-07, (Baltimore: STScI).
- Bohlin, R.C. 2000, AJ, 120, 437.
- Bohlin, R. C., Dickinson, M. E., & Calzetti, D. 2001, AJ, 122, 211.
- Bohlin, R. C. & Hartig, G. 1998, STIS ISR 98-20, (Baltimore: STScI).
- Davies, J. & Mobasher, B. 2003, STIS ISR (in progress), "Fullfield Sensitivity of STIS Imaging MAMAs", (Baltimore: STScI).
- Robinson, R. D. 1997, STIS IDT SMOV Report 044, "Examining the STIS Point Spread Function".